Science Advances
AAAS

advances.sciencemag.org/cgi/content/full/5/12/eaax9484/DC1

Supplementary Materials for

High-resolution cryo-EM structures of respiratory complex I: Mechanism, assembly, and disease

Kristian Parey, Outi Haapanen, Vivek Sharma, Harald Köfeler, Thomas Züllig, Simone Prinz, Karin Siegmund, Ilka Wittig, Deryck J. Mills, Janet Vonck, Werner Kühlbrandt, Volker Zickermann*

*Corresponding author. Email: zickermann@med.uni-frankfurt.de

Published 11 December 2019, *Sci. Adv.* **5**, eaax9484 (2019)
DOI: 10.1126/sciadv.aax9484

The PDF file includes:

Other Supplementary Material for this manuscript includes the following:

(available at advances.sciencemag.org/cgi/content/full/5/12/eaax9484/DC1)

Movie S1 (.mp4 format). Cryo-EM structure of respiratory complex I from *Y. lipolytica* in LMNG at 3.2-Å resolution.
Movie S2 (.mp4 format). Cryo-EM structure of ΔNDUFS4 at 4.0-Å resolution.
Movie S3 (.mp4 format). Cryo-EM structure of the ΔNDUFS6 assembly intermediate at 3.3-Å resolution.

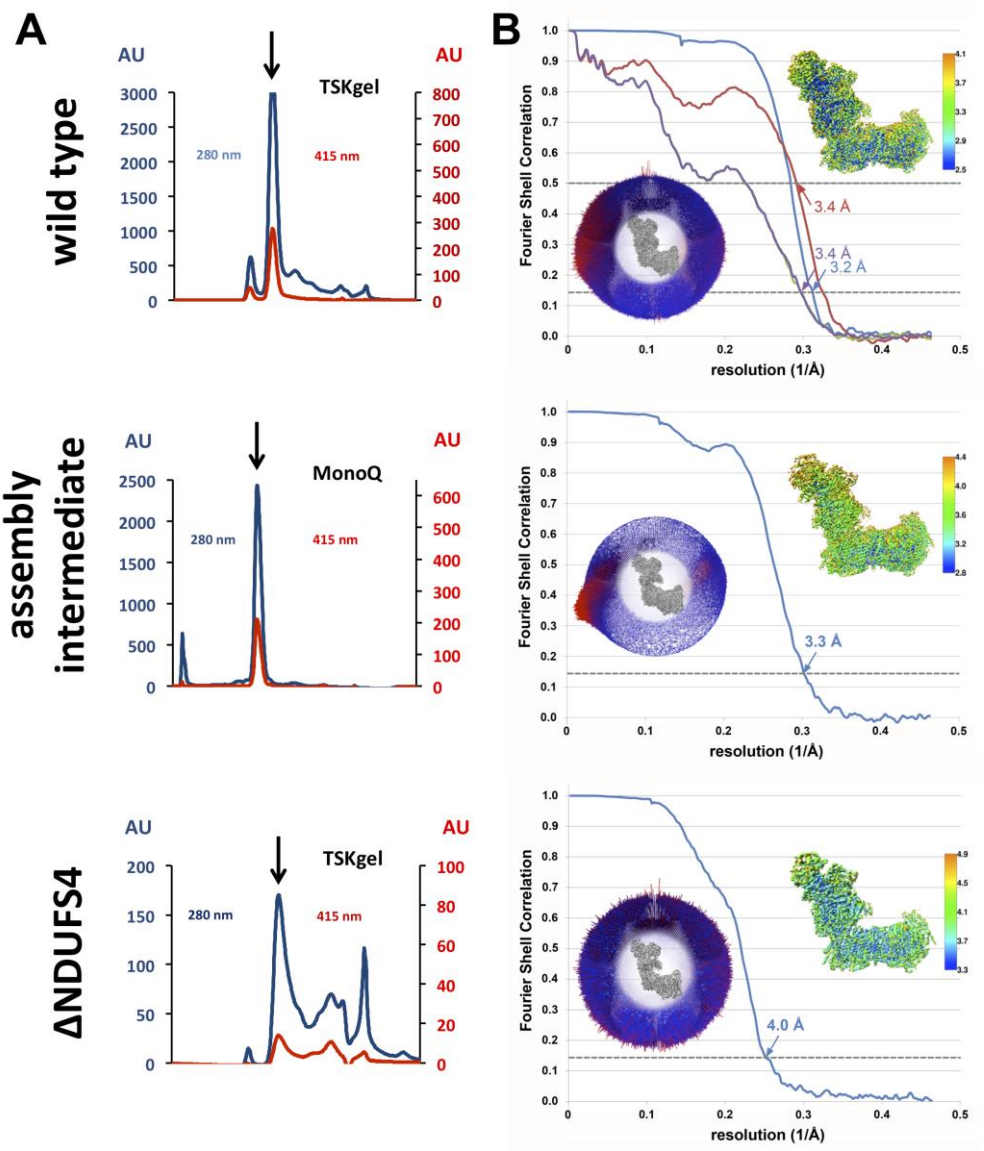

Fig. S1. Structure determination of wild-type complex I, assembly intermediate, and mutant without NDUFS4. A. Protein purification, column profile of final chromatography step. **B.** FSC plots for resolution estimation and model validation. Gold-standard FSC plots between two separately refined half-maps are shown in blue. The map resolution is indicated by the point where the curve drops below the 0.143 threshold (*51*). The FSC curve between the final refined model and the reconstruction of wild-type complex I from all particles (red) indicates a resolution of 3.4 Å (0.5 FSC criterion). FSC between the model refined in the reconstruction from half the particles and the reconstruction from that same half (FSC_{work}, purple), and between this model and the reconstruction from the other half of the particles (FSC_{free}, green) both indicate the same resolution, indicating that the model was not overfitted to the map. Inset left: Angular distribution plots of particle images. The number of particles with their respective orientation is shown by length and color of the cylinders. Inset right: cryo-EM maps of complex I colored by local resolution as analyzed by ResMap (*50*).

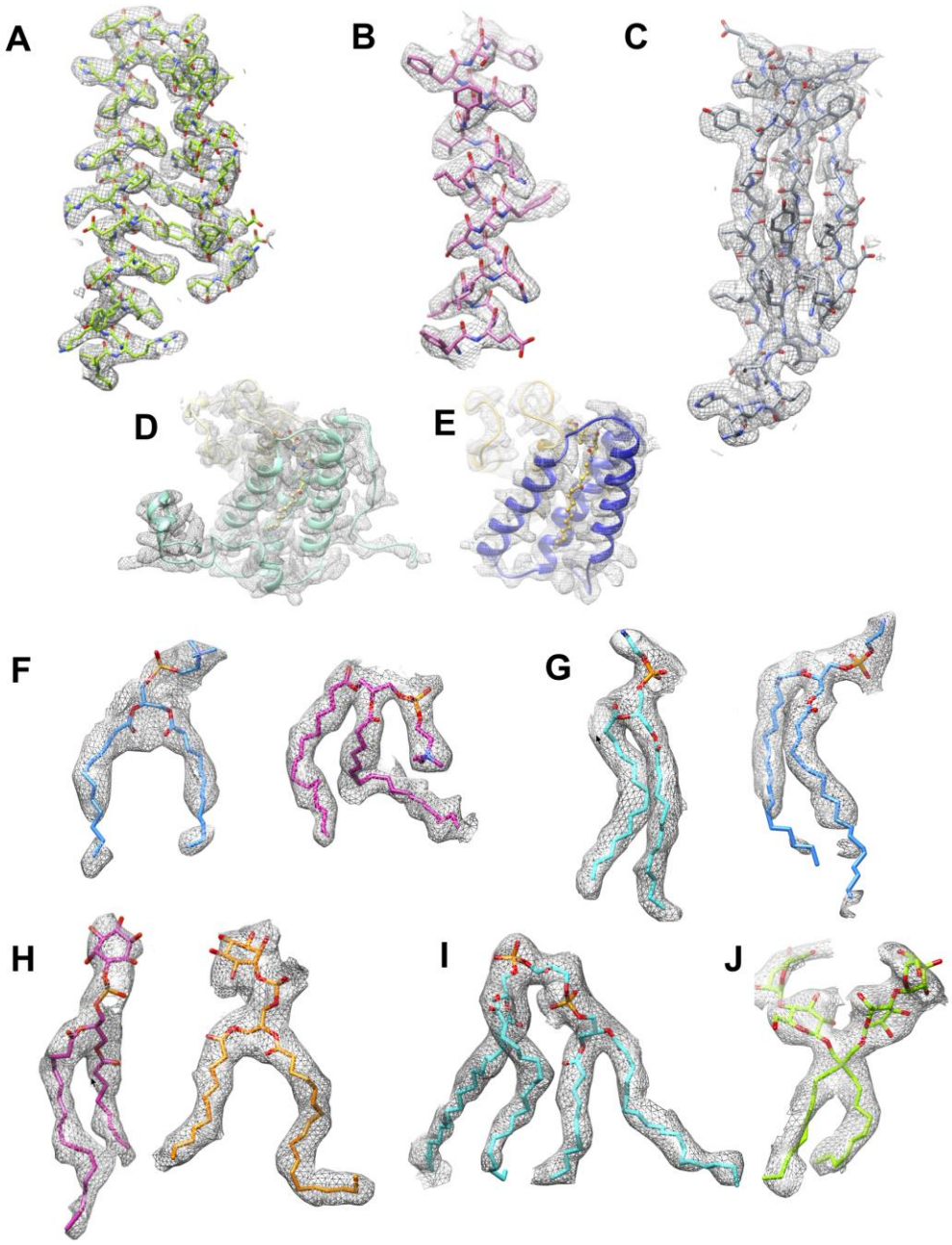

Fig. S2. Representative cryo-EM densities of wild-type complex I with fitted models. The map was sharpened with a B factor of -66 Å^2. **A.** Helix hairpin 167-220 in NDUFS2 in the peripheral arm. **B.** Transmembrane helix 273-293 of ND1. **C.** β-sheet 167-220 of NDUFS3. **D.** A region of the accessory LYR protein subunit NDUFA6; the acyl chain appended to the phosphopantetheine group of the adjacent acyl carrier protein ACPM1 (NDUFAB1) inserts into the interior of NDUFA6. **E.** Same as D for subunits NDUFB9 and ACPM2 (a second copy of NDUFAB1 in mammalian complex I. F-I: Lipid densities: **F.** Phosphatidylcholine (101 chain 5, 601 chain 2); **G.** Phosphatidylethanolamine (901 chain 4, 1001 chain 5); **H.** Phosphatidylinositol (501 chain 2, 201 chain 6); **I.** Cardiolipin (601 chain 4). **J.** LMNG detergent molecule (301 chain J). Ligand numbering as in PDB id: 6RFR.

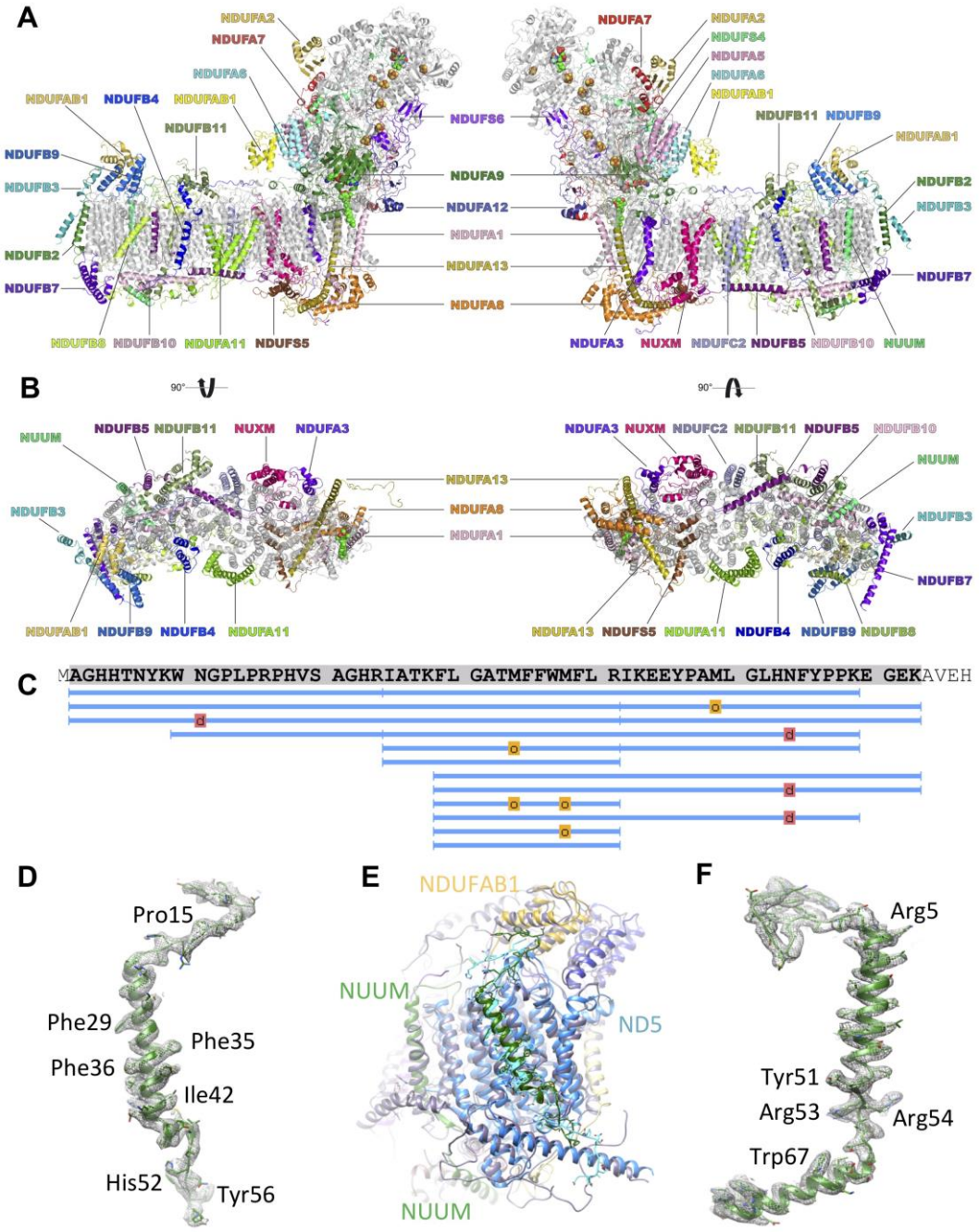

Fig. S3. Assignment of accessory subunits. Central subunits are shown in grey, accessory subunits are labeled and colored. **A.** Side views. **B.** View from the matrix (left) and from the intermembrane space (right) with peripheral arm subunits removed for clarity. **C.** Mass spectrometry identified 10 peptides matching to NIGM with a protein coverage of 93%. Blue lines represent peptides identified for NIGM (FDR <0.01), including peptides with variable modification o (methionine oxidation) and d (deamidation of asparagine and glutamine). **D.** Model of subunit NIGM in the cryo-EM density. **E.** Overlay of *Y. lipolytica* (colors as in A, some subunits labeled) and mouse (purple, PDB id: 6G2J) complex I. NIGM is dark green and mouse NDUFB2 cyan, with side chains. Subunit NB2M/NDUFB3 is omitted for clarity. **F.** Model of subunit NUUM in the cryo-EM density.

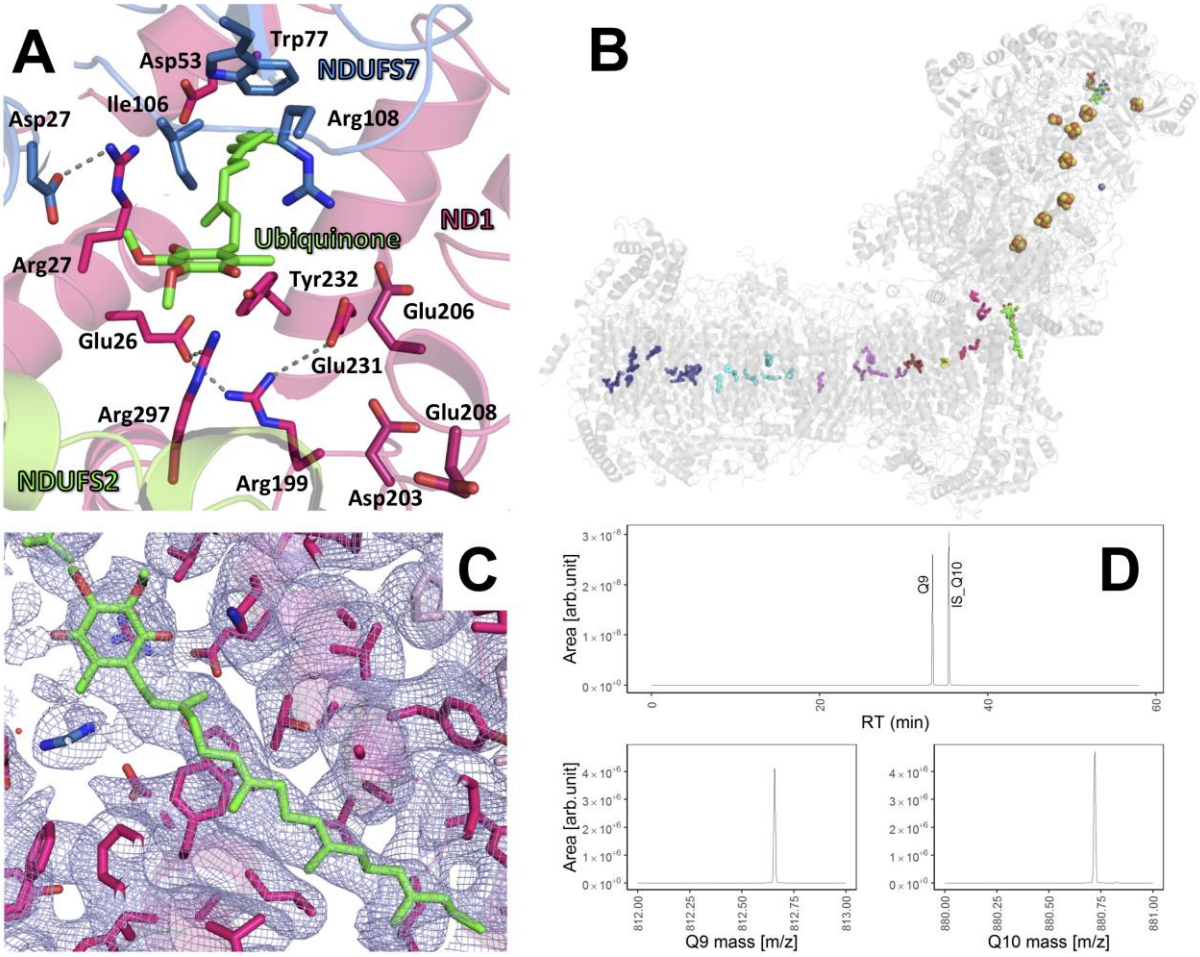

Fig. S4. A second Q binding site in complex I and quantitative mass spectrometry. The Q binding site newly identified in this work is different from the Q reduction site close to FeS cluster N2 (*8*). **A.** View from FeS cluster N2 towards the membrane. The Q head group is surrounded by several charged residues of ND1 (hot pink) and NDUFS7 (blue) that form an ion pair network; the side chain of hydrophobic Ile106 of NDUFS7 points to the center of the head group (see also figs. S4 and S5). Residues Asp203, Glu206, and Glu208 form the end of the hydrophilic axis (*6, 7*) that connects to the pump elements in the membrane arm. **B.** chain of conserved basic and acidic residues ("hydrophilic axis", colors) connects the ion pair network in the Q access tunnel and the newly identified second Q binding to the proton pumping modules in the membrane arm. An electron transfer step at the second Q binding site is hypothetical but would place Q redox chemistry in immediate contact to the hydrophilic axis (see ref. (*18*)). **C.** Q molecule with surrounding residue side chains shown as stick models. Density map drawn at 1.0 σ contour level in blue mesh. **D.** A coenzyme Q9 and internal standard Q10 (IS_Q10) from wild-type *Y. lipolytica* complex I extract. The area of the extracted ion chromatogram was used for quantification. **Insets.** The monoisotopic mass of the protonated ammonium adduct of Q9 (B) and IS_Q10 (C) with 2.7 ppm and 2.2 ppm mass deviation from theoretical monoisotopic mass and the retention time was used for identification.

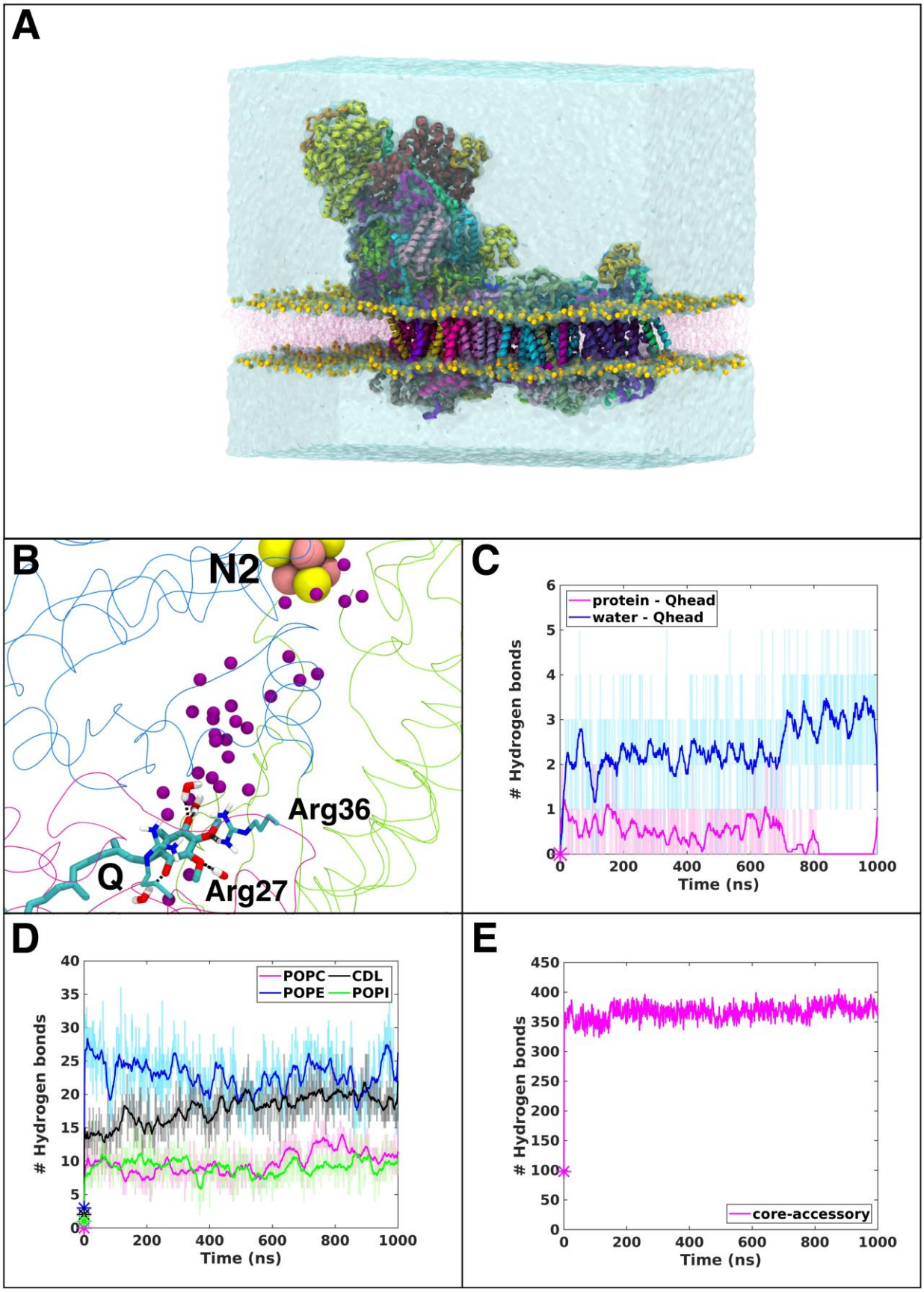

Fig. S5. Atomic model of *Y. lipolytica* complex I in membrane-solvent environment and hydrogen bond analysis from MD simulation trajectory. A. An atomic model (at time = 0 ns) of *Y. lipolytica* complex I comprising ca. 1.3 million atoms. Protein subunits are colored as in

Fig. 1. Phosphate groups of the lipid head groups are shown as yellow spheres and the lipid tails in transparent pink. Water molecules forming the simulation box are shown in cyan surface representation. Ions are omitted for clarity. Note that the figure shows the state at the start of the production simulation. **B.** A simulation snapshot (at 528 ns) shows hydration of the Q binding pocket. The space between FeS cluster N2 and Q head group is filled with water molecules (purple spheres). Hydrogen bonds between the Q head group, water molecules and residue $Arg36^{ND1}$ are displayed with black dotted lines. Q and residues $Arg27^{ND1}$ and $Arg36^{ND1}$ are shown as sticks, whereas the subunits NDUFS2, ND1 and NDUFS7 are shown as green, dark pink, or blue ribbons. In order to reach the Q reduction site near N2, the Q molecule must displace water molecules, which would contribute to entropic cost. **C.** Hydrogen bonds between the Q head group, protein and water. During simulation the Q head group makes several hydrogen bonds with water molecules and protein residues. Overall, a greater number of hydrogen bonds are formed between the Q head group and water molecules, and fewer are made within the protein (see also panel B and main text). **D,E.** The increase in number and stabilization of protein-lipid and protein-protein hydrogen bonds indicate stability of the structure and simulation. Panel D indicates the hydrogen bonds between the protein and the structurally resolved lipids, differentiated by lipid type (PC, PE, cardiolipin and PI). Panel E shows the hydrogen bonds between the functional core of the enzyme and the accessory subunits with respect to simulation time. In all three panels (C, D and E), asterisks show the number of hydrogen bonds present in the original structural conformation. In C and D panels, the data was smoothened by a running average, whereas the original data is shown as a shadow behind the trace. Hydrogen bonding criteria used in this analysis are donor (D) – acceptor (A) distance of below 3.5 Å and D-H angle above 150°.

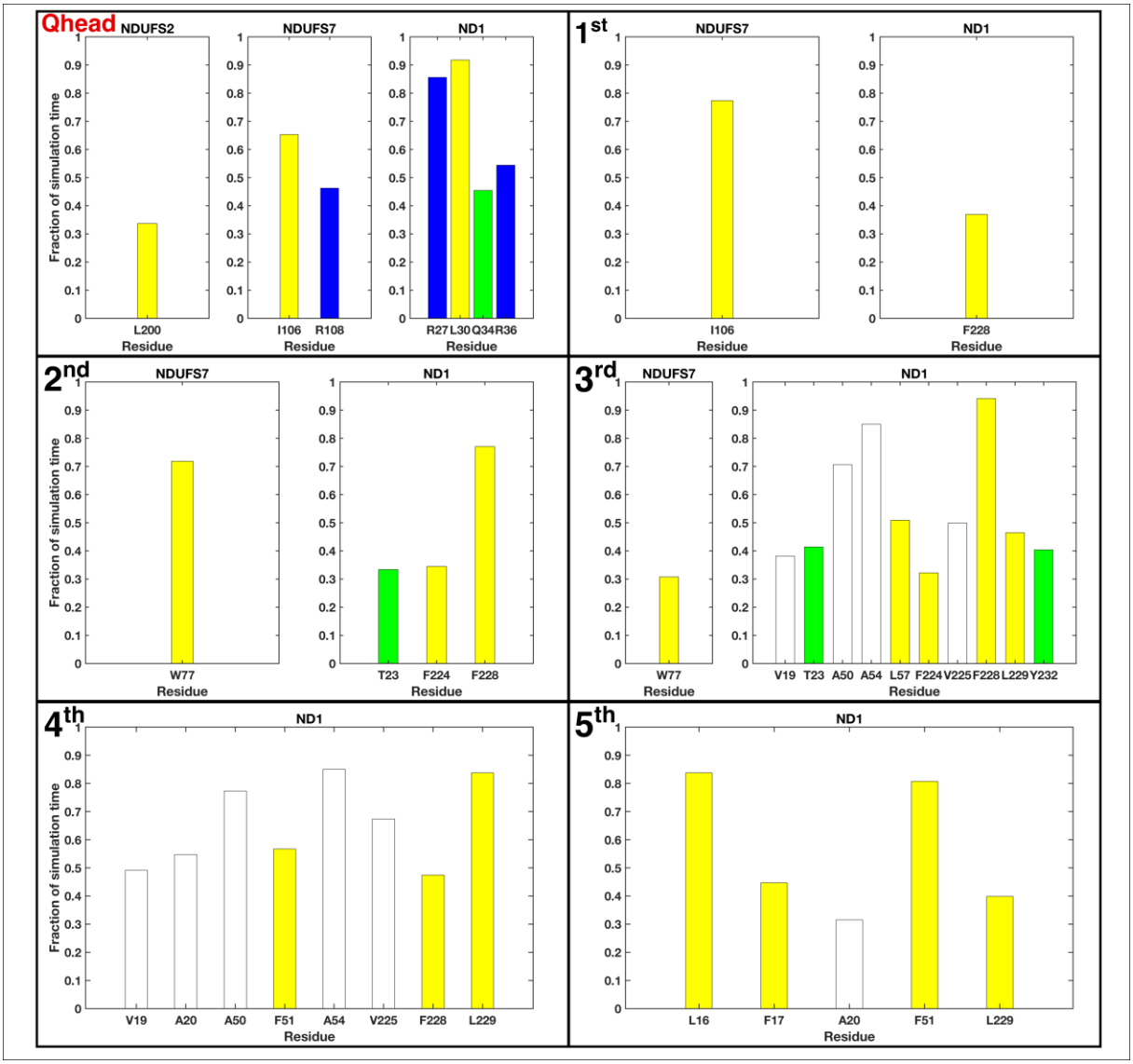

Fig. S6. Interactions between protein and the Q head group and tail. The interactions of protein residues with the Q head group (Qhead) and the first five isoprenoid units (1st, 2nd, 3rd, 4th and 5th) are shown as the fraction of simulation time (value of 1 on the y-axis means the contact existed for the entire simulation time of 1 μs). The Q head group makes significant contacts to residues Ile106^{NDUFS7}, Arg108^{NDUFS7}, Arg27^{ND1} and Arg36^{ND1} in agreement with the structural data. Similarly, the Q tail makes contact to residues Trp77^{NDUFS7}, Ala50^{ND1}, Ala54^{ND1}, and Tyr232^{ND1} (see main text). The contact data are differentiated based on the subunit type and residue type (yellow - hydrophobic, white - aliphatic, green - polar and blue - basic). Only interactions that existed for longer than 30% of the simulation time are reported and criteria for counting a contact were defined as a distance below 3 Å between Q (head group or selected isoprenoid unit) and the amino acid side chain. For the isoprenoid units, only contacts with non-polar residues were analyzed. Note that exchange of the corresponding residue of Ala54 in human ND1 is one of the most prevalent mutations causing Leber´s hereditary optic neuropathy (*74*).

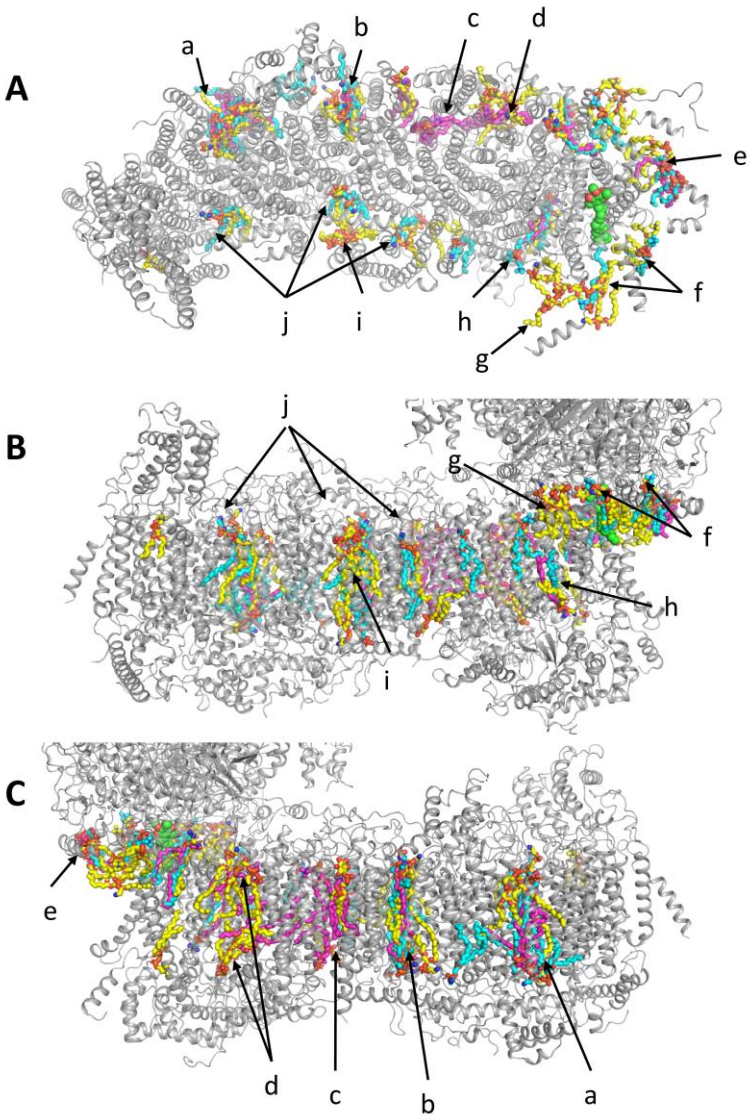

Fig. S7. Lipid binding sites in yeast and mammalian complex I. A. top view. **B, C.** side views of the membrane arm of *Y. lipolytica* complex I (protein, grey cartoon; 33 bound lipids, yellow sticks; Q molecule in second binding site, green spheres) overlaid with the membrane arms of mouse complex I (PDB id: 6G2J, 20 bound lipids, cyan sticks) and ovine complex I (PDB id: 5LNK, 12 bound lipids, magenta sticks). Lipid binding between ND5/ND4 (a), ND4/ND2 (b), ND6/ND1 (h) and to amphipathic helices of NDUFS8, NDUFA12 and NDUFA7 (e) is consistently observed in all three structures (*14*, *21*). An extended lipid-binding site in ovine complex I (c) (*14*) is occupied by the first three TMH of yeast ND2 that are lacking in mammalian complex I. Two lipid molecules flanking the first helix of NDUFS7 (f) and lipid-binding sites close to the ND5 lateral helix (j) are present in mouse (*21*) and yeast complex I. Cardiolipin is thought to be essential for complex I function (*14*, *21*, *75*, *76*). Therefore, sites (a) and (e) are especially interesting as they consistently comprise cardiolipin molecules. Further cardiolipin molecules are bound to NUXM/ND2 (d), NDUFA9 (g) and between accessory subunit NDUFA11 and the lateral NU5M helix (i) in *Y. lipolytica* complex I.

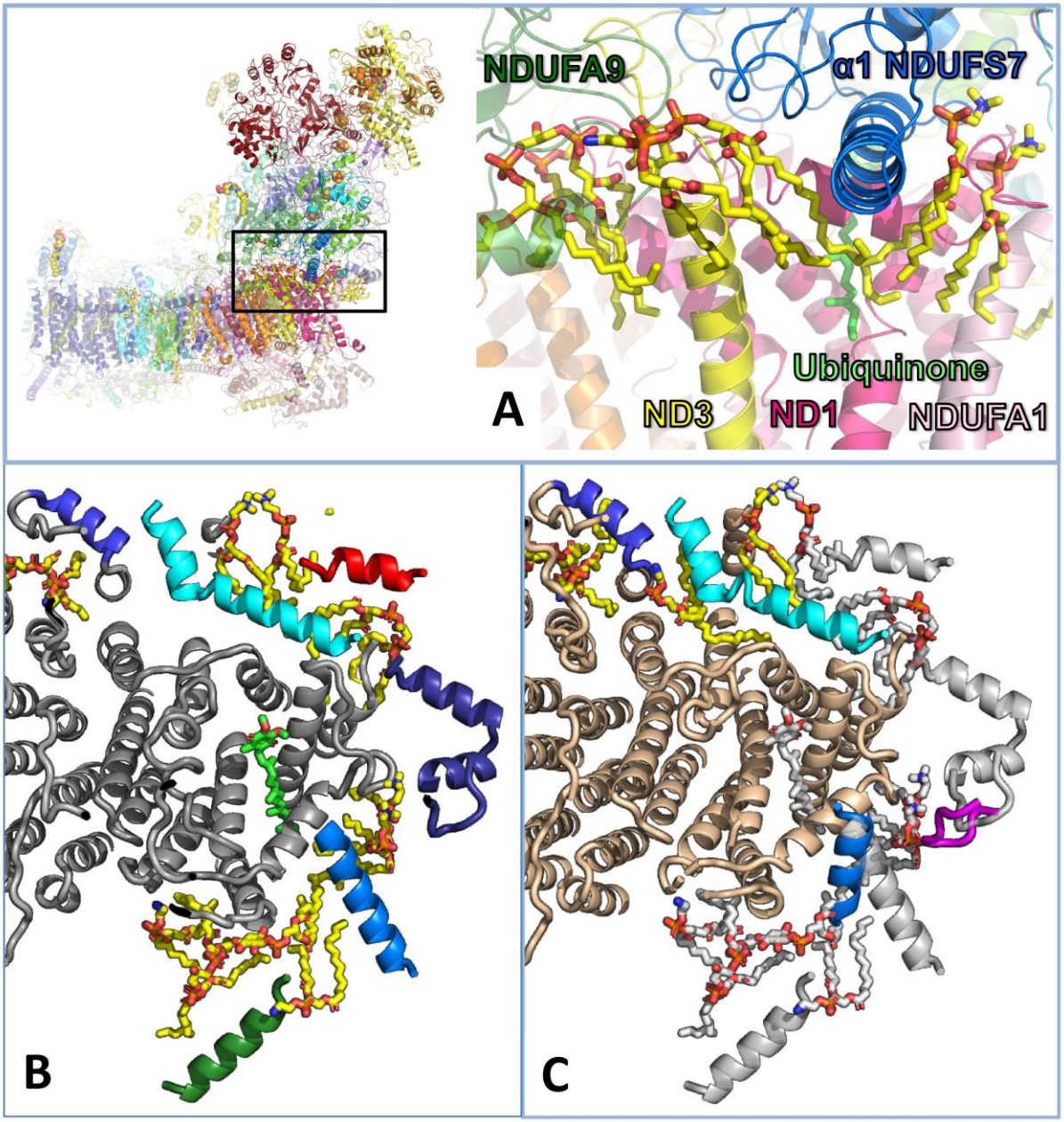

Fig. S8. Surface helices and lipids modeled at the interface of the membrane arm and the peripheral arm. A. Interface region in side view, helix α1 of NDUFS7 is situated above the entry portal for Q and is packed by four lipid molecules with tilted tails. **B.** Interface region in top view with peripheral arm removed, the interface is lined by amphipathic surface helices of subunits NDUFA9 (green), NDUFS7 (marine), NDUFA12 (dark blue), NDUFS8 (cyan), NDUFA7 (red) and NDUFA3 (blue). Modeled lipids (yellow) and Q (green) are shown in stick representation. **C.** Same view as (B) for the assembly intermediate. Assembly factor NDUFAF2 (magenta) is present, helix 1 of NDUFS7 is shifted, and density for several surface helices and lipids is missing (grey), indicating disorder.

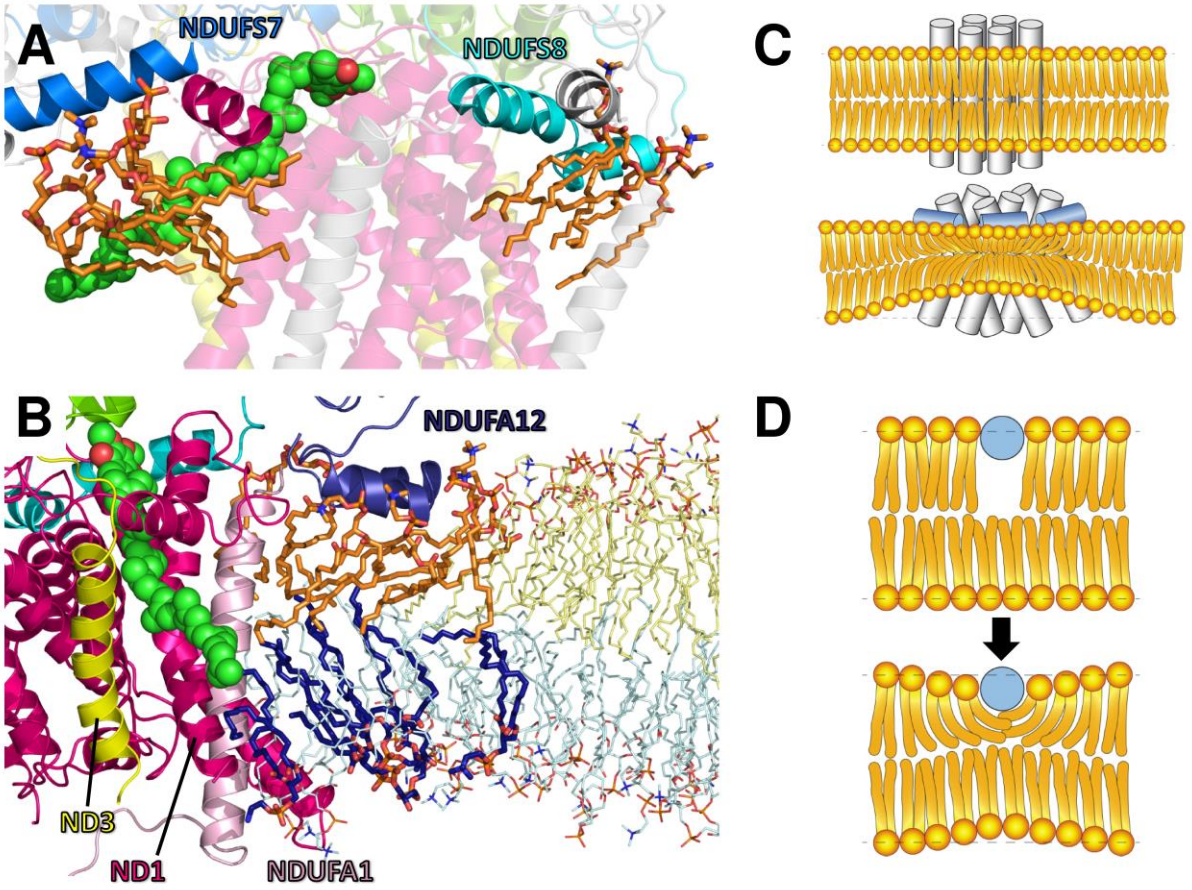

Fig. S9. Bending of the lipid tails seen in MD simulation. A. Slice view from the back of the membrane / matrix arm interface with selected lipids in stick representation. Bent lipid tails wrap around the hydrophobic side of amphipathic surface helices from core and accessory subunits. **B.** Side view of the membrane / matrix arm interface; lipid tails in the matrix side leaflet (orange) bend more than those in the opposite leaflet (dark blue), whereas lipid tails further away from the protein surface are straighter (yellow and cyan thin sticks). In panels (A) and (B), Q is shown as spheres (carbon – green and oxygen – red), core subunits are colored and accessory subunits are grey. **C.** Amphipathic surface helices generate locally reduced bilayer thickness. When TM helices are aligned normal to the lipid bilayer and when no amphipathic helices are present, the lipid tails are oriented more or less in line with the membrane normal (above); amphipathic surface helices at the membrane / matrix arm interface (fig. S8) displace the lipid head groups and destabilize the lipid tail region (below); the space required by lipid head group increases as TMHs become tilted relative to the membrane normal. **D.** Distortion of the default lipid geometry by adsorption of a single amphipathic helix; adapted from Fig. 7 in (*22*).

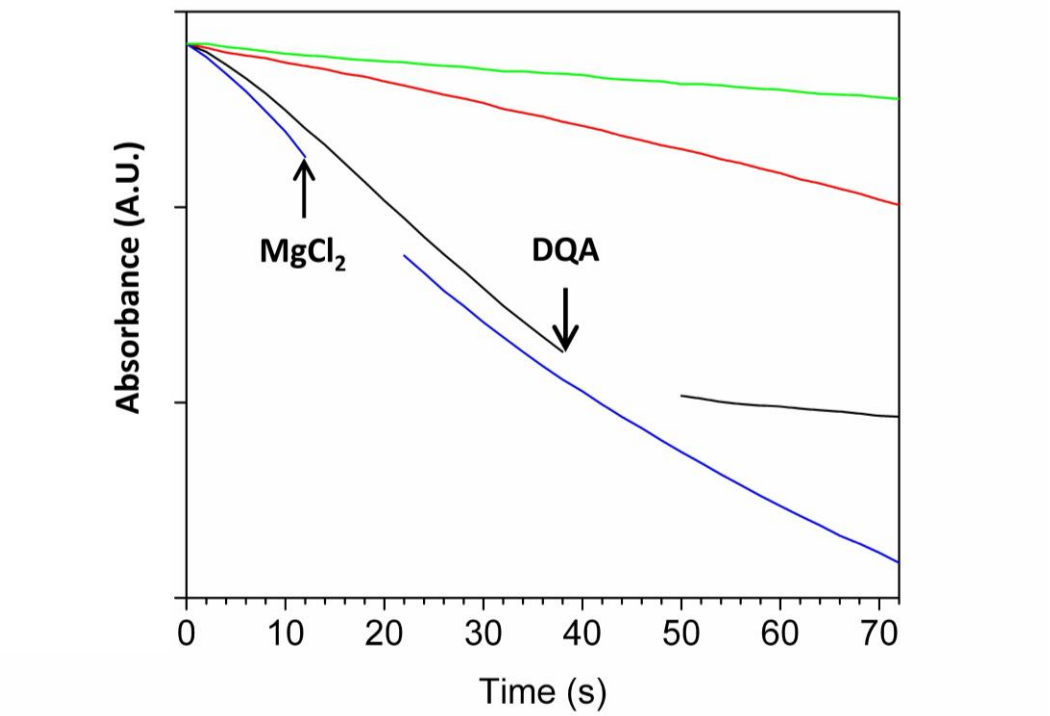

Fig. S10. Spectrophotometric assay of NADH:DBQ activity (*73*). The reaction was started by addition of NADH (time point 0) and monitored at 340 nm; data points during mixing are not shown; black: complex I without pretreatment (control), addition of inhibitor DQA at indicated time point; green: complex I pretreated with 2 mM NEM, NEM reacts exclusively with the D form that is irreversibly arrested by modification of a conserved cysteine residue in the loop connecting TMH1 and 2 of ND3; red: complex I pretreated with 5 mM $MgCl_2$, 5 mM $MgCl_2$ in assay buffer; blue: complex I without pretreatment, addition of 5 mM $MgCl_2$ at indicated time point. The D form of complex I is stabilized by Mg^{2+}. Addition of Mg^{2+} after conversion to the A form by turnover has no effect, in contrast to addition of Mg^{2+} before start of the reaction. The combined data prove that purified complex I from *Y. lipolytica* is in the D form.

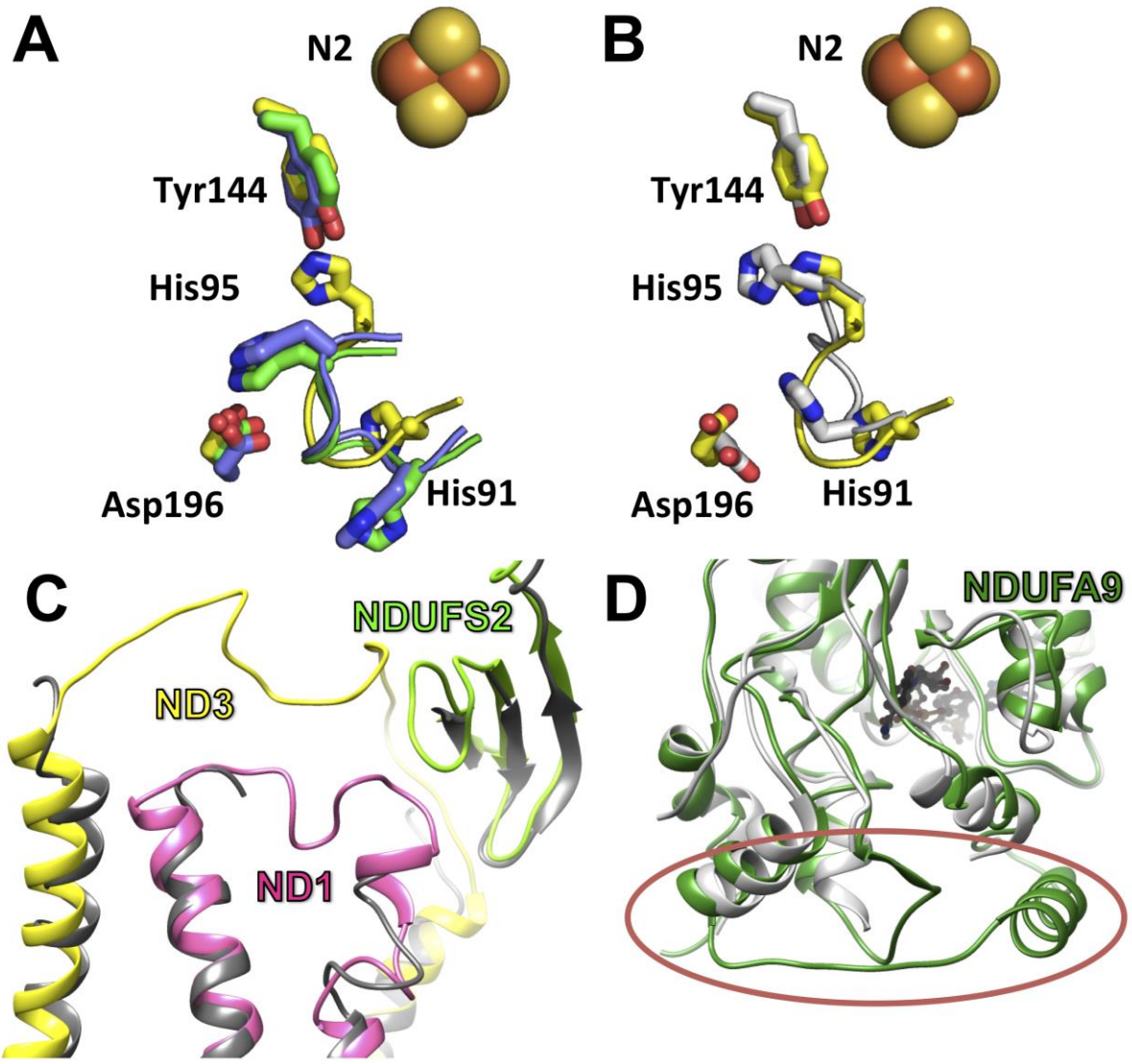

Fig. S11. Conformation of the β1-β2 loop of NDUFS2 and loops and regions critical for the active/deactive transition. A. Overlay of the NDUFS2 loop of *Y. lipolytica* complex I in the deactive form (X-ray structure, PDB id: 4WZ7, yellow; cryo-EM structure, PDB id: 6RFR, green) with the corresponding loop of mouse complex I in the active form (cryo-EM structure, PDB id: 6G2J, blue). In the X-ray structure the side chain of His95 points towards Tyr144 near FeS cluster N2; in the cryo-EM structure the same residue interacts with Asp196 in the four-helix bundle of NDUFS2. **B.** Overlay of *Y. lipolytica* X-ray structure with ovine complex I (grey, PDB id: 5LNK). In both cases complex I was analyzed in the presence of polyoxyethylene detergents (Thesit or Brij-35). Different detergents used for purification might explain the difference in loop conformation between the X-ray (Thesit) and cryo-EM (LMNG) structure of *Y. lipolytica* complex I. **C.** Overlay of *Y. lipolytica* complex I in LMNG (color) with the corresponding structure of mouse complex I in the deactive form (PDB id: 6G72, grey). Loops between TMHs 1 and 2 in ND3, TMHs 5 and 6 in ND1, β1 and β2 in the NDUFS2 subunit. **D.** The unfolded region of NDUFA9 in mouse complex I is marked by a red ellipse.

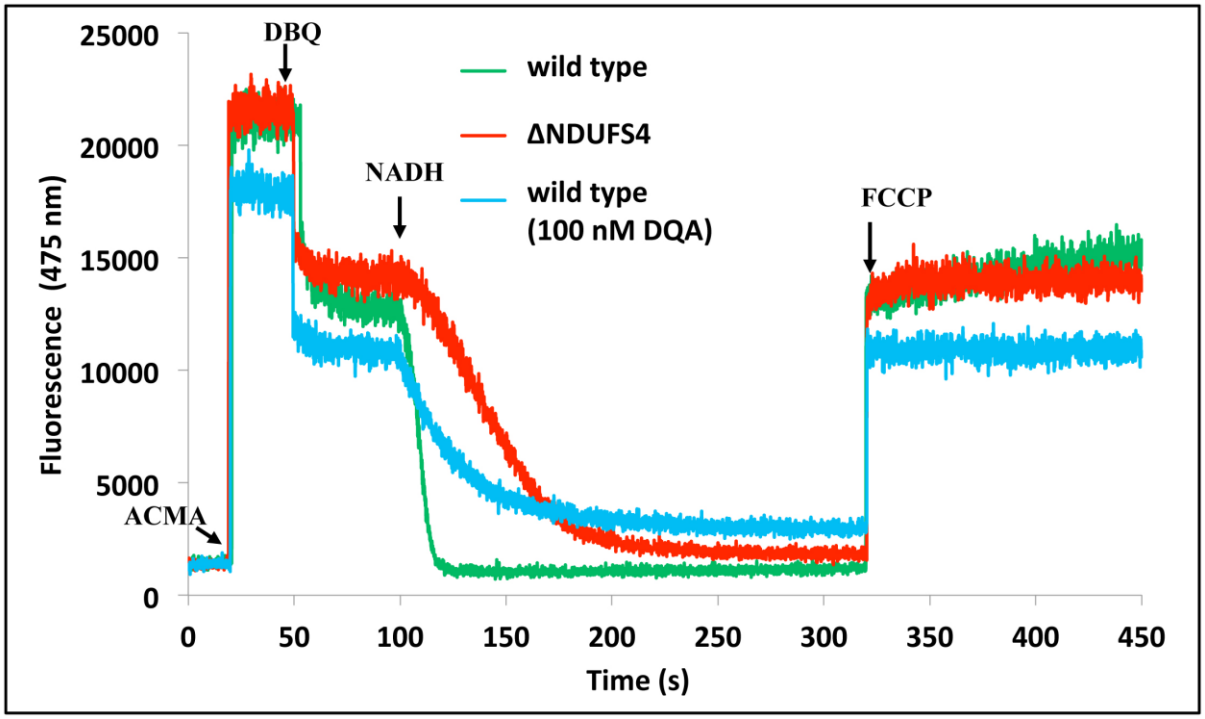

Fig. S12. Proton pumping activity of the NDUFS4 mutant. Proton pumping was monitored as 9-amino-6-chloro-2-methoxyacridine (ACMA) fluorescence quench in proteoliposomes. At time points indicated, 0.5 μM ACMA, 60 μM decylubiquinone (DBQ), 100 μM NADH and 5 μM of the uncoupler trifluoromethoxy carbonylcyanide phenylhydrazone (FCCP) were added during the assay. Wild type showed the same electron transfer activity as the mutant at 100 nM concentration of the inhibitor DQA.

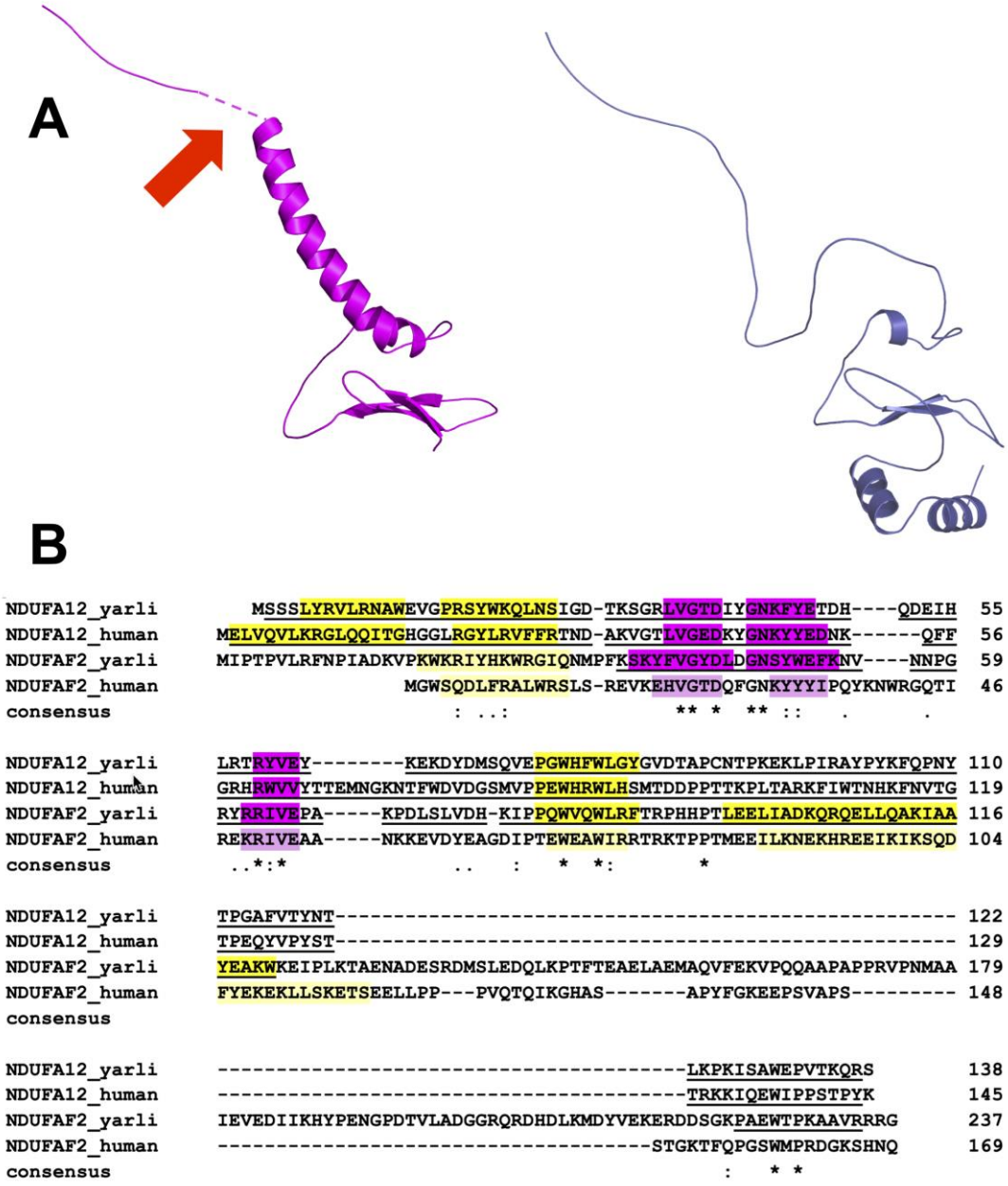

Fig. S13. Cartoon representation and sequence alignment of NDUFAF2 and NDUFA12 from *Y. lipolytica* and *Homo sapiens*. A. NDUFAF2 (magenta) and NDUFA12 (blue) in cartoon representation, the arrow highlights a stretch of unresolved sequence. **B.** Structure-based alignment of NDUFA12 and NDUFAF2. *Y. lipolytica* NDUFA12: chain h of PDB id: 6RFR; human NDUFA12: chain N of PDB id: 5XTB (*77*); *Y. lipolytica* NDUFAF2: chain k of PDB id: 6RFQ. Modelled sequence is underlined. α-helices observed in the structures are highlighted in bright yellow, β-strands in bright pink. Helices and strands predicted with the JPred4 server (*78*) are light yellow and light pink, respectively.

Table S1. Data collection, refinement, and model statistics.

	wild type	assembly intermediate	ΔNDUFS4
Data collection			
Microscope	FEI Titan Krios	FEI Titan Krios	FEI Tecnai Polara
Camera	Gatan K2 Summit	Gatan K2 Summit	Gatan K2 Summit
Voltage (kV)	300	300	300
Nominal magnification	125,000x	125,000x	200,000x
Calibrated pixel size (Å)	1.077	1.077	1.09
Electron exposure ($e^-/Å^2$)	42.2 - 50.0	50.0	60.0
Exposure time total (s)	8	8	8
Number of frames per image	40	40	40
Defocus range (μm)	1.5 - 2.5	1.5 - 2.5	2.0 - 3.0
Image processing			
Motion correction software	*MotionCor2*	*MotionCor2*	*MotionCor2*
CTF estimation software	*CTFFIND4*	*CTFFIND4*	*Gctf*
Particle selection software	*RELION3.0*	*RELION3.0*	*RELION3.0*
Final micrographs	4043	1386	5964
Initial particle images (no.)	666,666	250,406	418,740
Final particle images (no.)	297,066	112,418	145,767
Applied *B*-factor ($Å^2$)	-66	-50	-30
Final resolution (Å)	3.2	3.3	4.0
Refinement statistics			
Modeling software	*COOT, PHENIX*	*COOT, PHENIX*	*COOT, PHENIX*
Protein residues	8057	7637	7685
Ligands	49	36	12
Map CC (volume)	0.75	0.73	0.83
RMS deviations			
Bond lengths (Å)	0.0119	0.0132	0.0105
Bond angles (°)	1.55	1.65	1.46
Average B-factor ($Å^2$)	30.1	61.3	159.8
Ramachandran plot			
Outliers (%)	0.11	0.15	0.18
Allowed (%)	6.00	7.03	8.31
Favored (%)	93.89	92.82	91.51
Rotamer outliers (%)	0.16	0.17	0.15
Molprobity score	1.86	1.95	1.98
All-atom clashscore	8.36	9.29	8.89
PDB ID	6RFR	6RFQ	6RFS

Table S2. Subunit names, and chain identifiers for *Y. lipolytica* and human and bovine complex I.

Y. lipolytica	Human	Bovine	chain	total	wild type	assembly intermediate	ΔNDUFS4
central subunits							
NUAM	NDUFS1	75 kDa	A	694	692	694	692
NUBM	NDUFV1	51 kDa	B	470	456	441	456
NUCM	NDUFS2	49 kDa	C	444	438	430	387
NUGM	NDUFS3	30 kDa	G	251	239	210	239
NUHM	NDUFV2	24 kDa	H	216	216	215	213
NUIM	NDUFS8	TYKY	I	198	190	190	190
NUKM	NDUFS7	PSST	K	183	177	153	170
NU1M	NU1M	ND1	1	341	340	318	340
NU2M	NU2M	ND2	2	469	469	469	469
NU3M	NU3M	ND3	3	128	127	108	116
NU4M	NU4M	ND4	4	486	486	486	486
NU5M	NU5M	ND5	5	655	654	654	632
NU6M	NU6M	ND6	6	185	183	183	138
NULM	NULM	ND4L	L	89	89	89	83
accessory subunits peripheral arm[1]							
NUEM	NDUFA9	39 kDa	E	355	349	263	331
NUFM	NDUFA5	B13	F	136	121	121	121
NUMM	NDUFS6	13 kDa	M	119	117	-	117
NUYM	NDUFS4	18 kDa	Y	137	123	123	-
NUZM	NDUFA7	B14.5a	Z	182	181	120	181
N7BM	NDUFA12	B17.2	h	137	136	-	136
NB4M	NDUFA6	B14	P	123	123	123	123
ACPM1	NDUFAB1	SDAP	O	84	77	77	77
NI8M	NDUFA2	B8	f	86	80	79	80
accessory subunits P_P module							
NUPM	NDUFA8	PGIV	U	171	171	171	171
NUJM	NDUFA11	B14.7	J	197	179	179	116
NB6M	NDUFA13	B16.6	W	122	121	119	121
NIPM	NDUFS5	15 kDa	9	88	86	86	66
NUXM	-/-	-/-	X	168	167	168	167
NI9M	NDUFA3	B9	g	87	76	76	76
NIMM	NDUFA1	MWFE	D	86	86	86	86
NEBM	NDUFC2	B14.5b	b	73	64	64	64

accessory subunits P_D module							
NESM	NDUFB11	ESSS	S	204	174	174	174
NIAM	NDUFB8	ASHI	a	125	124	124	124
NUNM	NDUFB5	SGDH	n	119	114	114	113
NB2M	NDUFB3	B12	c	59	44	44	44
NB5M	NDUFB4	B15	j	92	90	90	90
NB8M	NDUFB7	B18	8	98	82	82	80
ACPM2	NDUFAB1	SDAP	Q	88	85	85	85
NIDM	NDUFB10	PDSW	d	91	90	90	90
NI2M	NDUFB9	B22	R	108	106	106	106
NUUM	-/-	-/-	i	89	83	83	83
NIGM	NDUFB2	AGGG	e	67	52	52	52
assembly factor							
N7BML	NDUFAF2	NDUFAF2	k	237	-	98	-
No. of residues				8300	8057	7637	7685

[1]accessory subunit ST1 is a substoichiometric component of *Y. lipolytica* complex I; complex I was purified from a strain carrying a deletion of the ST1 gene to improve sample homogeneity (compare Materials and Methods)

Table S3. Lipid species detected in *Y. lipolytica* complex I. Lipid species detected in *Y. lipolytica* complex I. PC, PE, PS, and LPC were analyzed as $[M+H]^+$ ions in positive mode. PI and CL as $[M-H]^-$ ions in negative mode. Precursor mass (MS1) was used for quantification and MS2 fragment ions or retention time (RT) for identification.

nmol/nmol complex I	Lipid Species	MS1 Precursor m/z	Δ m/z (ppm)	RT (min)	MS2 Fragment	Fragment Name
0.48	PC 33:2	744.5568	4.0854	21.69	184.07	PC Head
0.65	PC 34:1	760.5872	2.7296	24.58	184.07	PC Head
2.52	PC 34:2	758.5715	2.7699	22.92	184.07	PC Head
1.78	PC 34:3	756.5568	4.0206	21.12	184.07	PC Head
0.66	PC 35:2	772.5872	2.6872	24.01	184.07	PC Head
1.48	PC 35:3	770.5715	2.7268	22.32	184.07	PC Head
0.39	PC 35:4	768.5558	2.6872	20.6	184.07	PC Head
1.93	PC 36:2	786.6017	1.2884	25.07	184.07	PC Head
8.62	PC 36:3	784.5872	2.6461	23.46	184.07	PC Head
9.83	PC 36:4	782.5705	1.3591	21.73	184.07	PC Head
Σ 28.3	PC					
0.27	PE 32:1	690.5069	0.0945	22.67	549.49	NL_PE Head
0.44	PE 33:1	704.5245	2.9159	23.82	563.50	NL_PE Head
0.44	PE 33:2	702.5089	2.9599	22.1	561.49	NL_PE Head
2.39	PE 34:1	718.5382	0.1060	24.94	577.52	NL_PE Head
4.34	PE 34:2	716.5235	1.4190	23.28	575.50	NL_PE Head
1.36	PE 34:3	714.5079	1.4580	21.53	573.49	NL_PE Head
0.74	PE 35:2	730.5402	2.8613	24.37	585.49	NL_PE Head
0.80	PE 35:3	728.5245	2.8198	22.67	587.50	NL_PE Head
1.68	PE 36:2	744.5538	0.0686	25.42	603.53	NL_PE Head
5.12	PE 36:3	742.5402	2.8151	23.78	601.52	NL_PE Head
3.35	PE 36:4	740.5245	2.7741	22.1	599.50	NL_PE Head
Σ 20.9	PE					
0.26	PS 34:1	762.5300	2.7123	22.35	577.52	NL_PS Head
0.18	PS 34:2	760.5144	2.7524	20.6	575.50	NL_PS Head
0.12	PS 36:4	784.5123	0.0230	23.4	601.52	NL_PS Head
Σ 0.6	PS					
0.009	LPC 16:0	496.3407	1.9389	4.16	184.07	PC Head
0.005	LPC 16:1	494.3241	0.0219	2.81	184.07	PC Head
0.004	LPC 17:0	510.3554	-0.0172	5.41	184.07	PC Head
0.038	LPC 18:1	522.3566	2.2033	4.88	184.07	PC Head
0.053	LPC 18:2	520.3409	2.1427	3.41	184.07	PC Head
0.007	LPC 21:0	566.4181	0.1308	11.74	184.07	PC Head
Σ 0.1	LPC					
0.30	PI 33:1	821.5216	3.7167	20.8	241.01	PI Head
0.39	PI 33:2	819.5060	3.7564	18.98	241.01	PI Head
2.12	PI 34:1	835.5342	0.0449	21.96	241.01	PI Head
3.03	PI 34:2	833.5186	0.0751	20.23	241.01	PI Head

0.95	PI 34:3	831.5040	1.2799	18.42	241.01	PI Head
0.20	PI 35:1	849.5509	1.2360	23.12	241.01	PI Head
0.66	PI 35:2	847.5352	1.1965	21.42	241.01	PI Head
0.62	PI 35:3	845.5166	-2.3081	19.64	241.01	PI Head
0.77	PI 36:2	861.5509	1.2188	22.55	241.01	PI Head
1.50	PI 36:3	859.5344	0.1857	20.83	241.01	PI Head
1.28	PI 36:4	857.5186	0.0730	19.05	241.01	PI Head
Σ 11.8	PI					
0.59	CL 63:4	1329.8838	-2.1891	36.22		
0.22	CL 70:4	1427.9983	1.4287	37.85		
0.43	CL 70:5	1425.9806	-0.0069	37.14		
1.24	CL 70:6	1423.9680	2.1538	36.36		
1.17	CL 70:7	1421.9514	1.4877	35.6		
0.34	CL 70:8	1419.9347	0.7337	34.85		
0.20	CL 71:5	1439.9962	-0.0243	37.56		
0.58	CL 71:6	1437.9806	-0.0069	36.82		
0.77	CL 71:7	1435.9650	0.0106	36.04		
0.61	CL 71:8	1433.9495	0.1132	35.31		
1.20	CL 72:5	1454.0129	0.7143	37.93		
4.09	CL 72:6	1451.9983	1.4051	37.24		
2.66	CL 72:7	1449.9767	-2.7008	36.46		
4.32	CL 72:8	1447.9650	0.0105	35.72		
0.22	CL 72:9	1445.9493	0.0278	34.99		
0.16	CL 73:10	1457.9464	-1.9819	36.04		
0.55	CL 74:9	1473.9786	-1.3318	37.24		
0.73	CL 74:10	1471.9640	-0.6531	36.5		
1.06	CL 74:11	1469.9464	-1.9657	35.72		
Σ 21.1	CL					
Σ 82.8	all lipids					

Movie S1. Cryo-EM structure of respiratory complex I from *Y. lipolytica* in LMNG at 3.2-Å resolution. Subunits are colored as in Fig. 1.

Movie S2. Cryo-EM structure of ΔNDUFS4 at 4.0-Å resolution. Subunits are colored as in Fig. 1.

Movie S3. Cryo-EM structure of the ΔNDUFS6 assembly intermediate at 3.3-Å resolution. Subunits are colored as in Fig. 1.